Intermediate-velocity atomic collisions. VI. Screening, antiscreening, and related processes in $He^+ + (H_2, He)$

E. C. Montenegro and W. S. Melo
Departamento de Física, Pontifícia Universidade Católica do Rio de Janeiro, Caixa Postal 38071, Rio de Janeiro, 22453-900, Rio de Janeiro, Brazil

W. E. Meyerhof
Department of Physics, Stanford University, Stanford, California 94305-4060

A. G. de Pinho
Instituto de Física, Universidade de São Paulo, Caixa Postal 20516, São Paulo, 05508-900, São Paulo, Brazil
(Received 14 June 1993)

The total electron loss, target ionization, and simultaneous projectile-target ionization are measured for He^+ projectiles on H_2 and He in the energy range of 1.5–4.0 MeV. The experimental data are in good agreement with calculations based on the independent-particle model including screening, antiscreening, and target-ionization probabilities as well as second-order mechanisms for the simultaneous projectile-target ionization.

PACS number(s): 34.50.Fa

I. INTRODUCTION

This work continues our previous studies of atomic collisions in the intermediate-velocity regime [1–5]. Our present aim is to obtain a detailed survey of the mechanisms that are responsible for the electron loss of one-electron projectiles in the vicinity of the cross-section maximum.

The theoretical basis for the quantal description of the electron-loss process for projectiles colliding with neutral targets was established by Bates and Griffing [6] about 40 years ago. The theory is based on the plane-wave Born approximation (PWBA) and includes the contributions from the target nucleus as well as from the target electrons as the perturbing sources responsible for the projectile electron loss. Due to the inclusion of the electron-electron interaction, the mutual excitation (or ionization) of the projectile and the target plays an important role in the theory, making it necessary to consider all the possible excited states of the target in order to determine the total cross section for the electron loss. This sum over the final target excited states can be carried out for atomic hydrogen targets, but is difficult to perform for more complex targets, such as multielectron atoms or molecules. For this reason, further approximations are introduced in the theory, the simplest being the closure approximation [7,8]. This approximation strongly simplifies the calculations of the cross section for the electron loss, since it requires only knowledge of the target-ground-state form factor. Unfortunately, the closure approximation gives very poor results when compared with the exact Bates-Griffing theory or experiment [9].

The electron-electron interaction can play either a passive or an active role during the projectile electron-loss process. If the target atom remains in the ground state during the collision, the target electrons screen the target nuclear potential in a passive way. This has been called the screening mode [8]. If the target electrons are excited or ionized, they become active ionization agents, with the nucleus assuming a passive role. This mode has been called antiscreening [8].

If the antiscreening contribution to projectile electron loss is evaluated by the closure approximation, some important dynamical features of the electron-electron interaction are not taken into consideration. This fact was first identified by Anholt [9] who introduced an *ad hoc* correction to the antiscreening contribution in order to take into account the onset of the electron-electron interaction when the translational kinetic energy of the target electrons in the projectile frame becomes high enough to ionize the projectile. A different approach was proposed by Hartley and Walters [7] with the assumption that target ionization is the predominant mode of excitation and using closure only indirectly to assure the proper behavior of the total cross section at high velocities. Montenegro and Meyerhof [10], through an extended sum-rule method, derived the onset of the antiscreening mode directly from the PWBA and Meyerhof *et al.* [11] considered the effects related to molecular targets in the cross sections. The results of the diverse methods were compared with experiment for several collision systems [5,12], giving excellent general agreement. It is important to note that these improvements of the closure method affect only the *antiscreening* part of the electron-loss cross section and, as a consequence, change the total cross section for electron loss through the change of the *relative* contributions of the screening and antiscreening modes. This last observation also applies to the calculation of Ref. [13], where the antiscreening contribution is calculated through the Impulse Approximation whereas the screening contribution is calculated by the PWBA.

It has been shown recently by Montenegro and Meyerhof [14,15], through the development of the semiclassical approximation (SCA) of electron loss, that the screening and the antiscreening processes act at different internuclear distances. Because these two processes also obey different collision dynamics, possible second-order effects can affect differently the screening and the antiscreening modes, changing their relative contribution to electron loss. For these reasons, it is important to measure separately the screening and the antiscreening modes in order to have a more stringent verification of the theoretical calculations than the total cross section can provide.

This paper reports measurements of the total cross section for projectile electron loss, target single ionization, and simultaneous projectile and target ionization for $He^+ + (H_2, He)$ collisions within the 1.5–4.0 MeV energy range. A comprehensive interpretation of these data in terms of the recently developed PWBA and SCA theories for the electron loss [10,14,15] is given, showing that calculations based mainly on first-order perturbation theories give a satisfactory description of the electron loss and related processes in the intermediate-velocity regime.

II. EXPERIMENTAL PROCEDURE AND RESULTS

Figure 1 shows a general sketch of the experimental arrangement. A He^+ beam with energies from 1.5 to 4.0 MeV is delivered by the 4-MV Van De Graaff accelerator of the Catholic University of Rio de Janeiro, which, before entering the experimental line, is energy and charge analyzed. After suitable collimation, the beam enters into the gas cell where it undergoes charge changing collisions in He or H_2. Two different charge states (He^+ and He^{2+}) of the emergent beam are charge analyzed by a second analyzing magnet and recorded by two surface-barrier detectors housed in a detection chamber. Target recoil ions (He^+ or H_2^+) produced by the primary beam are detected by a microchannel plate after being accelerated by an 800-V electric potential.

The accelerating potential is applied to the recoil ions in two stages. The first stage consists of a plate-grid system with the primary beam passing through the middle and with an applied voltage of 500 V. The second stage is an "Einzel" lens designed to focus the recoil ions into a 2-mm diam. aperture placed at the center of a time-to-flight tube. This aperture, together with two other 1.8-mm diam. apertures placed at the beam entrance and exit of the gas cell, assures a differential pressure ratio of 1/300 between the outer chamber and the gas cell, which is adequate for the microchannel plate operation. The distance between the two 1.8-mm aperatures is 6.5 cm, which gives 6.8 cm for the effective length of the cell [16].

At least five different pressures, up to 5 mTorr, are used in singles measurements to obtain the total cross section for projectile electron loss by the growth-rate method. Further details of the procedure used in these measurements can be found in Ref. [5]. The coincidence events between the recoil ions and each emergent charge state are independently obtained by using two time-to-amplitude converters (TAC's) together with the associated standard fast electronics. Figures 2(a) and 2(b) show the recorded time spectra for 1.5-MeV He^+ collisions resulting in projectile electron loss. All the coincidence measurements are carried out at 1 mTorr. The overall efficiency of the recoil-ion detection system (solid angle, efficiency of the focusing system, and micro-channel

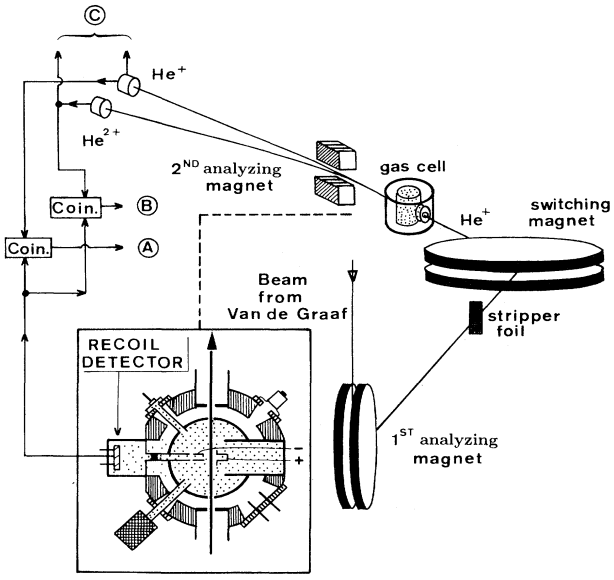

FIG. 1. Sketch of the experimental arrangement, with the target chamber in the inset.

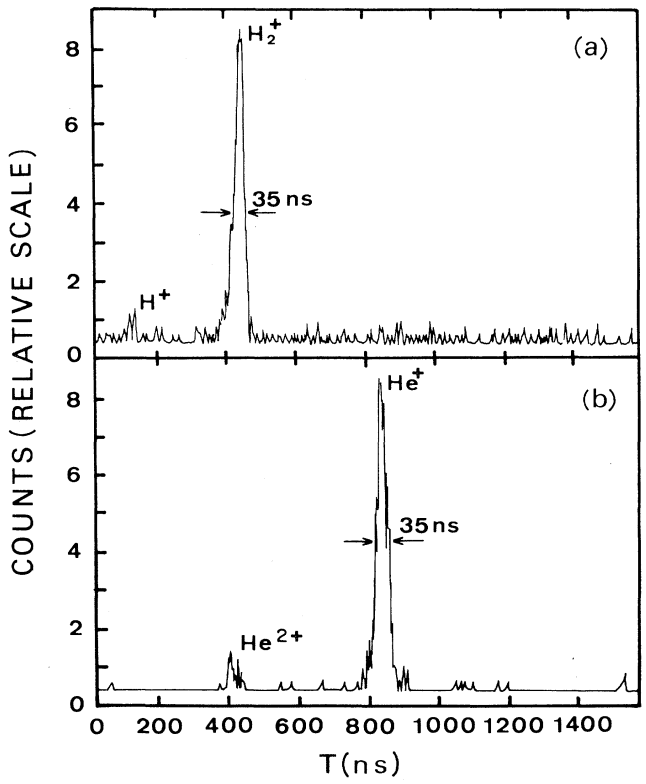

FIG. 2. Time spectra for the He^{2+} emerging projectiles in coincidence with singly charged recoil ions for 1.5-MeV He^+ projectiles on (a) H_2 and (b) He.

TABLE I. Measured cross sections for target ionization (TI), simultaneous projectile-target ionization (PTI), and total projectile electron loss (L) for H_2 and He targets. All cross sections are given in Mb. The PTI cross sections are taken from Ref. [29].

	H_2			He		
E (MeV)	TI	PTI	L	TI	PTI	L
1.5	111±11	12.2±1	22±3	75±4	11.2±0.8	20±3
1.8			15.6±2			17±2
2.0	89±9	9.2±1.0	15.3±2	56±3	7.3±0.5	16.6±2
2.5	77±8	8.4±0.9	13.4±1	49±3	6.8±0.5	12.5±1
3.0	87±9	7.7±0.8	11.6±1	43±2	5.9±0.4	11.4±1
3.5	60±6	7.3±0.8	9.7±1	42±2	5.2±0.4	10.2±1
4.0	53±5	5.1±0.6	7.5±0.8	36±2	4.9±0.4	8.7±0.9

plate) is obtained by measuring the target-ionization cross section (H_2^+ or He^+ recoils) by 2.0-MeV protons and using the values reported by Rudd *et al.* [17] for normalization.

With the above experimental arrangement and procedures, the cross sections for the following processes are measured:

(a) *Target single ionization (TI).* This process corresponds to the reaction

$$He^+ + (H_2, He) \rightarrow He^+ + (H_2^+, He^+) , \quad (1)$$

and is obtained by a coincident measurement of the singly ionized recoils with the He^+ emergent beam.

(b) *Simultaneous projectile and target single ionization (PTI).* This process corresponds to the reaction

$$He^+ + (H_2, He) \rightarrow He^{2+} + (H_2^+, He^+) , \quad (2)$$

and is obtained through the He^{2+} emergent beam coincidence branch.

(c) *Projectile electron loss (L).* This process is obtained through the singles measurement of emergent He^{2+} ions and corresponds to events resulting in projectile ionization irrespective of the final state of the target.

Table I presents our results. The main sources of uncertainties in the singles measurements (L) come from gas purity (~2%) background fluctuations (~2%) and the effective length of the cell (9–11 %). In the coincidence measurements (TI and PTI), the main uncertainties come from the normalization procedure, statistics, and random coincidence subtraction, and the overall uncertainties range between 13–15%.

III. TOTAL CROSS SECTION FOR PROJECTILE ELECTRON LOSS

Figures 3(a) and 3(b) compare our measurements of the one-electron-loss cross section with other experimental results and theoretical calculations for H_2 and He targets, respectively. The low- and intermediate-velocity data for H_2 are from Refs. [18–20]. For the He target, the data are from Refs. [19,21,22]. Our low-energy points are in excellent agreement with data of Sataka, Yagishita, and Nakai [20], DuBois [22], and Atan, Steckelmacher, and Lucas [21]. The results from Ref. [23] of He^+ on He cover the energy range studied in this paper but seem to be systematically low, as observed by the authors themselves, and are not included in this figure.

The theoretical calculations are based on the work of Montenegro and Meyerhof using the extended-sum-rule method [10]. This method gives the electron-loss cross section in terms of form factors for the target ground state, a virtue also met by the closure approximation [7–10]. The form factors were obtained from Salvat *et al.* [24] for He, and from Meyerhof *et al.* [11], for H_2. In the latter case, the Stewart molecular form factor was

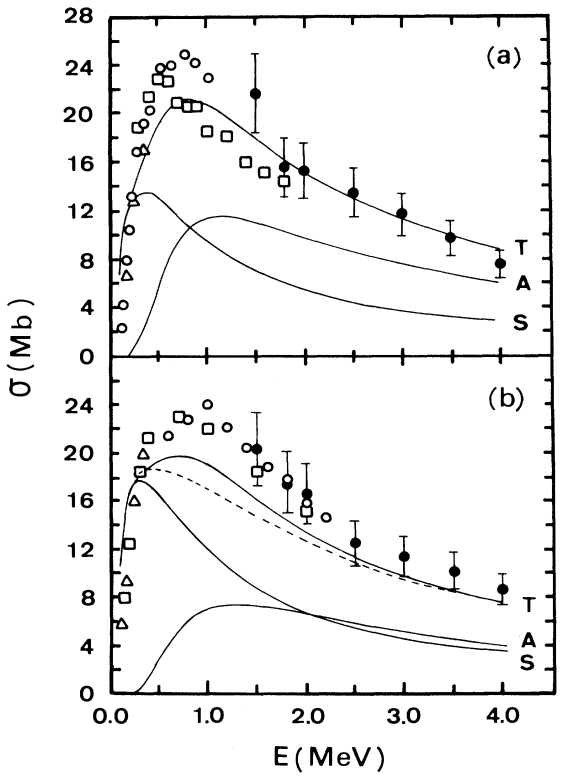

FIG. 3. Total He^+ electron-loss cross sections on (a) H_2 and (b) He. Theory: Curves S, A, and T correspond to calculated screening, antiscreening, and total (screening plus antiscreening) contributions, respectively; dashed curve, total-cross-section calculation from Ref. [25]. Experiment, H_2: solid circles, this work; open circles, Ref. [18]; open triangles, Ref. [19]; open squares, Ref. [20]; He: solid circles, this work; open triangles, Ref. [19]; open circles, Ref. [21]; open squares, Ref. [22].

used. These form factors appear in the antiscreening as well in the screening contributions to the electron-loss cross sections.

The curves labeled by S, A, and T in Figs. 3(a) and 3(b) represent the screening, antiscreening, and total cross sections, respectively, calculated as described above. Figure 3(b) also shows (dashed curve) the calculation of Bell, Dose, and Kingston [25] (length formulation) for the total-electron-loss cross section which can be considered "exact" within the PWBA framework. This calculation uses Hartree-Fock based wave functions to describe the excited (discrete and continuum) states of the He target and computes the total cross section through the sum of the calculated partial cross sections corresponding to these states, instead of using the closure relation. The present calculations agree well with those of Bell, Dose, and Kingston, giving a maximum 15% deviation in the vicinity of the cross-section maximum and corroborating our simpler calculation procedure based on the extended sum-rule method. There is good general agreement between the theoretical calculations and the present and previous measurements. Previous studies on the role of the screening-antiscreening effects in the electron loss were carried out in more asymmetric collision regimes [5,12,13]. Our results for the $He^+ + He$ system show that first-order calculations can be applied to symmetric collisions.

IV. TARGET IONIZATION CROSS SECTIONS

Figures 4(a) and 4(b) compare our mesaurements for target single-ionization cross sections with previous data of Edwards, Wood, and Ezell [26] and DuBois [22] for H_2 and He targets, respectively, showing good agreement between the present and previous data for both targets.

These figures also give a theoretical estimate for the target ionization cross section. Although the main subject of the present study is electron loss, the availability of a reasonable estimate for target ionization is important to show the consistency of our analysis as a whole, since target-ionization probabilities are needed for the calculation of coincidence cross sections associated with electron loss, as shown in the next section.

Our estimate for target ionization is carried out along the same lines as described in Ref. [5]. The cross section for *single*-electron target ionization is calculated within the independent-particle model as

$$\sigma_{\mathrm{TI}} = 4\pi \int_0^\infty db\, P_I(b)[1 - P_I(b)] \,, \tag{3}$$

where $P_I(b)$ is the one-electron ionization probability of the target (H_2 or He). The inadequacy of using first-order probabilities for the systems studied can be circumvented by the unitarization procedure proposed by Sidorovitch *et al.* [27]. Considering that the capture channel gives a negligible contribution, compared with the target ionization, for the systems studied, $P_I(b)$ is calculated as

$$P_I(b) = 1 - e^{-p_i(b)} \,, \tag{4}$$

where $p_i(b)$ is the first-order semiclassical ionization probability [28]. As in Ref. [5], $p_i(b)$ is calculated using

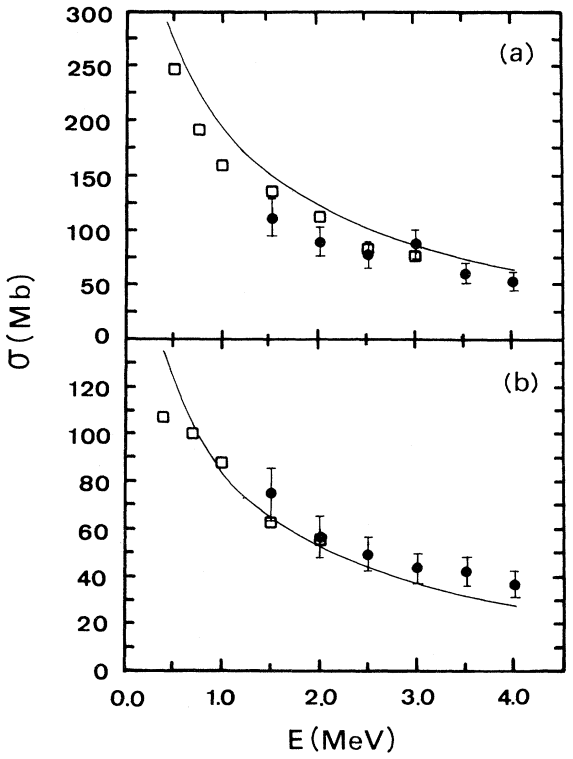

FIG. 4. Target-ionization cross sections on (a) H_2 and (b) He. Solid curve, theoretical calculations (see text). Experiment, H_2: solid circles, this work; open squares, Ref. [26]; He: solid circles, this work; open squares, Ref. [22].

$Z_{2K} = 1.19$, $\theta = 0.8$ and $Z_{2K} = 1.7$, $\theta = 0.586$ for H_2 and He targets, respectively, with the simplifying assumption that the incident He^+ ion can be considered as a bare projectile. Here, Z_{2K} is the internally screened target atomic number and θ is the external screening factor.

Besides its simplicity, the above procedure to calculate target *single* ionization agrees within 35% with the experimental data over the projectile energy range in Fig. 2, and for both targets. This result, to a certain extent, justifies the use of Eq. (4) and the independent-electron approximation in the analysis of more complex mechanisms, as is done below.

V. ANTISCREENING AND ASSOCIATED PROCESSES

Figures 5(a) and 5(b) display for H_2 and He, respectively, our coincidence measurements for simultaneous ionization of the projectile and the target, together with the data of DuBois [22] for the He case. These results have been discussed in Ref. [29] and are considered in greater detail here.

The measured cross sections, described by Eq. (2) result from the two different mechanisms, which are illustrated in Figs. 6(a) and 6(b). The mutual projectile-target ionization can occur via the electron-electron interaction (antiscreening) or via a second-order nucleus-electron interaction [two-center double ionization (DI)]. These two processes cannot be separated by the present kind of experiment. However, because they have a very different

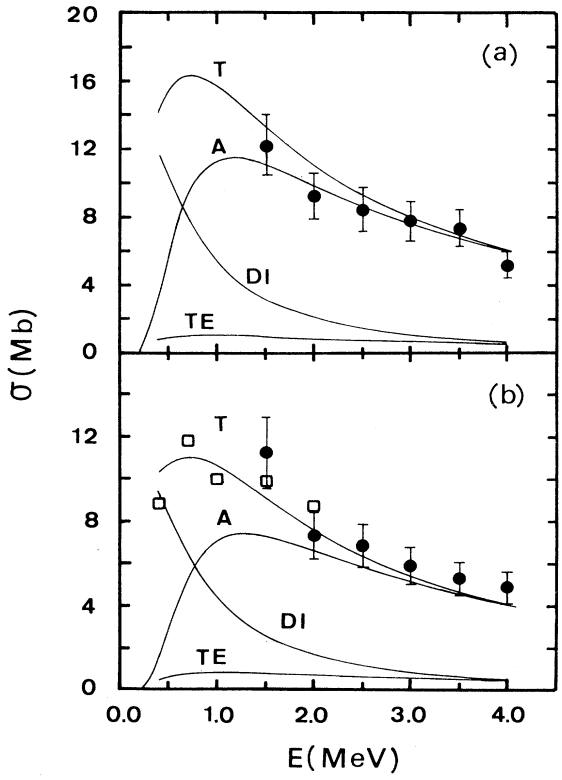

FIG. 5. Simultaneous target-projectile ionization cross section on (a) H_2 and (b) He. Theory: antiscreening (A), two-center double ionization (DI), projectile ionization-target excitation (TE), and total-cross-sections (T=A+DI−TE). Experiment, H_2: solid circles, Ref. [29]; He: solid circles, Ref. [29]; open squares, Ref. [22].

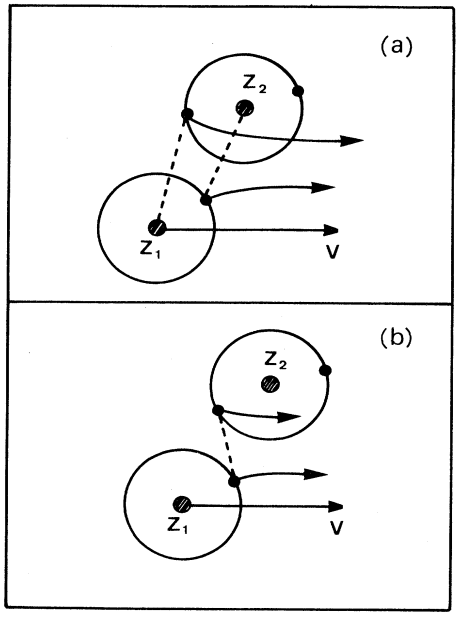

FIG. 6. Sketch of the (a) DI and (b) antiscreening contributions to the simultaneous projectile (Z_1)-target (Z_2) ionization.

physical origin it is possible to obtain a good understanding of the relative contributions of these two processes through the analysis of the energy dependence of the cross sections for each.

The calculation of the antiscreening contribution follows the procedure discussed in Sec. III. The corresponding curves for H_2 and He targets are labeled A in Figs. 5(a) and 5(b). This calculation is based on the extended sum-rule method of Ref. [10], which uses the closure approximation. As a consequence of this theoretical approach, not only the continuum, but also bound excited final target states are included in the calculation. However, excited target states are not included in the measurements since they do not produce recoil ions. A proper comparison between theory and experiment requires that the contribution from the target excited states be subtracted from the antiscreening calculations obtained through the closure approximation. Using the notation of Ref. [10], the contribution to antiscreening from target excitation can be written as

$$\sigma_{\mathrm{TE}}=\frac{8\pi Z_2}{(v/v_0)^2}\sum_{n\neq 0}\int_{q_0+q_n}^{\infty}dq\frac{1}{q^3}|F(q)|^2|\langle\phi_n|e^{-i\mathbf{q}\cdot\mathbf{r}}|\phi_0\rangle|^2 \tag{5}$$

where Z_2 is the target atomic number, v is the projectile velocity, $v_0=e^2/\hbar$ is the Bohr velocity, $q_0=(E_f-E_s)/\hbar v$, $q_n=(E_n-E_0)/\hbar v$, and $|\psi_s\rangle$ and $|\psi_f\rangle$ ($|\phi_0\rangle$ and $\phi_n\rangle$) are the initial and final states of the projectile (target) corresponding to energies E_s and E_f (E_0 and E_n), respectively.

The calculation of the transition matrix element $\langle\phi_n|e^{-i\mathbf{q}\cdot\mathbf{r}}|\phi_0\rangle$ was carried out using hydrogenic wave functions and the independent-electron approximation for the He target with an effective nuclear charge $Z_{\mathrm{eff}}=1.7$. The H_2 case was approximated by two hydrogen atoms. The sum over the final target states in Eq. (5) was considered for principal quantum numbers or up to 4. The results of these calculations are indicated by TE in Figs 5(a) and 5(b).

It can be seen from these figures that the contribution of target excitation to the total antiscreening cross section is small. In other words, when the projectile is ionized, the energy and momentum transferred to the projectile via electron-electron interaction make the (simultaneous) ionization of the target a more likely event than excitation, at least in the present collision systems. The electron-electron interaction results essentially in the ionization of both collision partners.

The DI process, which also can produce the events described by Eq. (2), can be viewed as a second-order screening collision. As illustrated in Fig. 6(a), DI corresponds to the double ionization of the projectile and the target by the simultaneous action of the screened nuclear potential of the target and the projectile, respectively. The cross section for this process can be estimated, using the independent-particle model, in the form

$$\sigma_{\mathrm{DI}}=4\pi\int_0^{\infty}db\,bP_{\mathrm{screen}}(b)P_I(b)[1-P_I(b)]\ . \tag{6}$$

The projectile-ionization probability $P_{\text{screen}}(b)$ is calculated using the theory of Ref. [14] and the target-ionization probability $P_I(b)$ is calculated using Eq. (4). Here, for simplicity, we also approximate H_2 by two hydrogen atoms.

The appropriateness of any $P_I(b)$ and $P_{\text{screen}}(b)$ used in Eq. (6) can be checked by calculating the target-ionization cross section through Eq. (3) and the screening cross section through

$$\sigma_{\text{screen}}=2\pi\int_0^\infty db\, bP_{\text{screen}}(b)\ , \tag{7}$$

and comparing this last result with the PWBA calculation (the target-ionization cross section is discussed in Sec. IV). With this procedure, the consistency of all the calculations can be ascertained.

The cross sections for the DI process calculated by Eq. (6) is labeled by DI in Figs. 5(a) and 5(b). This cross section has a strong energy dependence, decreasing in importance if compared with the antiscreening process, as the projectile energy increases. At lower projectile energies the relative importance of the DI process increases and, for projectile energies below the antiscreening threshold, is essentially the mechanism responsible for the mutual ionization of the projectile and the target.

The total cross section for the PTI reaction [Eq. (2)] is indicated by T (T=A−TE+DI) in Figs. 5(a) and 5(b) and is in very good agreement with our experimental results and those Ref. [22] for the He case, corroborating our theoretical procedures.

An important point to be noted from Figs. 5(a) and 5(b) is that, for the projectile energy range studied, there is an almost complete shift between the mechanisms resulting in the mutual projectile-target ionization as the projectile energy is varied. At low energies, a second-order *nucleus-electron* interaction dominates while at high energies, the *electron-electron* interaction (antiscreening) is the predominant mechanism. The difference between the dynamics of these two mechanisms is manifested in the impact parameter dependence of the corresponding probabilities. The probability for the DI process can be written as

$$P_{\text{DI}}(b)=2P_{\text{screen}}(b)P_I(b)[1-P_I(b)]\ , \tag{8}$$

in accord with Eq. (6). The probability $P_{\text{DI}}(b)$ is significant in the same range of impact parameters as $P_{\text{screen}}(b)$ or $P_I(b)$. On the other hand, the antiscreening probability $P_{\text{anti}}(b)$ has a much broader probability distribution, corresponding to the fact that this process is due to the interaction between two electron clouds [15]. In other words, DI can be associated with close collisions while antiscreening can be associated with distant collisions. This behavior can be seen in Figs. 7(a)–7(c), where the quantity $bP(b)$ for the antiscreening and DI processes in $He^+ + He$ collisions is shown as a function of the impact parameter b (in units of the Bohr radius a_0) for projectile energies of 0.5, 1.0, and 3.0 MeV, respectively. The DI and antiscreening probabilities, as well their sum, are indicated in these figures by DI, A, and T, respectively.

At 0.5 MeV, the projectile energy is just below the onset of the antiscreening process and DI clearly dominates. The pair of electrons is ejected by the two collision partners with an energy distribution which is characteristic of the nucleus-electron interaction, and the collision is essentially confined to impact parameters smaller than a_0 ($b<1$). At 1.0 MeV, the DI and antiscreening processes compete. The curve T shows a clear change near $b\sim 1$ as an indication of the presence of antiscreening at larger impact parameters. At 3.0 MeV, antiscreening is the dominant mechanism. The energy distribution of the ejected electrons is characteristic of the electron-electron interaction, and a significant part of the collisions resulting in the simultaneous target-projectile ionization now occurs at impact parameters larger than a_0.

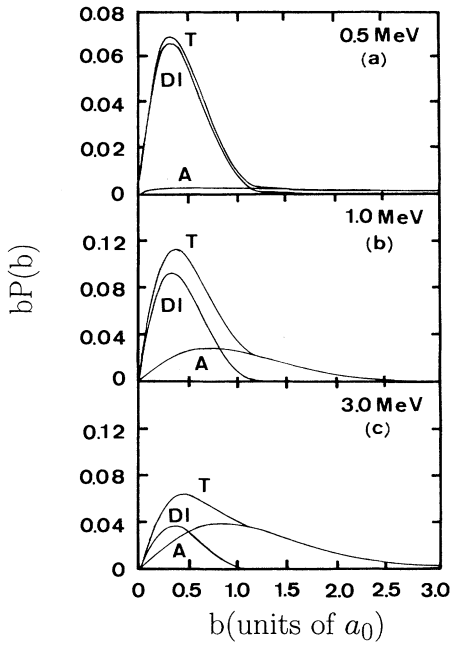

FIG. 7. Probability distribution $bP(b)$ as a function of the impact parameter for the antiscreening (A), two-center double ionization (DI), and total (T=A+DI) mechanisms in atomic units for (a) 0.5-MeV, (b) 1.0-MeV, and (c) 3.0-MeV He^+ projectiles on He.

From the above discussion, one can also justify our procedure to add the antiscreening and the DI processes incoherently in order to obtain the total cross section for the PTI reaction. In fact, because the DI and the antiscreening processes result in the same final electron states of the projectile and the target, the two processes should have been added coherently by summing their amplitudes instead of summing their probabilities, as was done. However, the two mechanisms have completely different dynamics, as reflected by the impact parameter dependence of the probability amplitudes and of the energy of the electrons in the continuum. Any interference term is expected to be small, since two amplitudes peak in different regions of the impact parameter and have different energy distributions for the ejected electrons. This occurs because the DI process is related to close collisions followed by large momentum transfer between the

target nucleus and the projectile electrons, but the antiscreening process is related to distant collisions and small momentum transfers.

VI. CONCLUSIONS

The main motivation for this work is to isolate the various mechanisms that are related to projectile electron loss in the intermediate-velocity regime. Basically, two kinds of interactions are important for the present study: the nucleus-electron interaction and the electron-electron interaction. The nucleus-electron interaction is responsible for the screening mode in the projectile electron loss and is the main mechanism leading to target ionization. Also, when projectile and target are simultaneously ionized, the second-order double-ionization process due to the simultaneous action of projectile and target nuclei on the target and projectile electrons, respectively, is the dominant mechanism at low projectile energies. On the other hand, the electron-electron interaction competes with the screening mode for the projectile electron loss, becoming the dominant mechanism for the simultaneous projectile-target ionization at high energies.

The present measurements of the total projectile electron loss of He^+ on H_2 and He show that the PWBA theory of Ref. [10] is in very good agreement with the experiment in the intermediate- to high-velocity regime, making evident the importance of the antiscreening contribution in correctly describing the total electron loss in these systems. Our new data also show that the PWBA approach can be extended to symmetric collision systems, a result which is possibly connected with the decrease of the target perturbing field because of the screening effect.

The measurements of target ionization extend the available data up to 4.0 MeV and show good overall agreement with the theoretical estimates performed within the independent-particle model. Although these estimates are not based on a first-principles approach, they provide consistency for the use of the independent-particle model in describing the second-order nucleus-electron interaction which results in the simultaneous projectile-target ionization.

Concerning the latter process, it is shown that both nucleus-electron (DI) and electron-electron (antiscreening) interactions must be considered to obtain a good agreement with experiment in the whole range of projectile energies studied. In fact, the good agreement attained between theory and experiment allows us to obtain a clear picture of this process in terms of the impact parameter dependencies of the two mechanisms. The connection of the DI and the antiscreening mechanisms with close and distant collisions, respectively, corroborates the analysis performed recently by various authors [30–35], relating the observation of low-energy electrons with the electron-electron interaction in electron loss. In fact, because distant collisions result in a smaller momentum transfer when compared with close collisions, low-energy electrons should be associated with the electron-electron interaction (antiscreening), while high-energy electrons should be associated with nucleus-electron collisions (DI) occurring preferentially in close collisions and resulting in large momentum transfers.

ACKNOWLEDGMENTS

This work was supported in part by CNPq (Brazil) and by National Science Foundation Grants No. INT-9101057 and No. PHY-9019293 (Stanford University).

[1] R. Anholt, X.-Y. Xu, Ch. Stoller, J. D. Molitoris, W. E. Meyerhof, B. S. Rude, and R. J. McDonald, Phys. Rev. A **37**, 1105 (1988).
[2] X.-Y. Xu, E. C. Montenegro, R. Anholt, K. Danzmann, W. E. Meyerhof, A. S. Schlachter, B. S. Rude, and R. J. McDonald, Phys. Rev. A **38**, 1848 (1988).
[3] E. C. Montenegro, X.-Y. Xu, W. E. Meyerhof, R. Anholt, K. Danzmann, A. S. Schlachter, B. S. Rude, and R. J. McDonald, Phys. Rev. A **38**, 1854 (1988).
[4] E. C. Montenegro, X.-Y. Xu., W. E. Meyerhof, and R. Anholt, Phys. Rev. A **38**, 3358 (1988).
[5] E. C. Montenegro, G. M. Sigaud, and W. E. Meyerhof, Phys. Rev. A **45**, 1575 (1992).
[6] D. R. Bates and G. Griffing, Proc. Phys. Soc. London, Sect. A **66**, 961 (1953); **67**, 663 (1954); **68**, 90 (1955).
[7] H. M. Hartley and H. R. J. Walters, J. Phys. B **20**, 1983 (1987).
[8] J. H. McGuire, N. Stolterfoht, and P. R. Simony, Phys. Rev. A **24**, 97 (1981).
[9] R. Anholt, Phys. Lett. A **114**, 126 (1986).
[10] E. C. Montenegro and W. E. Meyerhof, Phys. Rev. A **43**, 2289 (1991).
[11] W. E. Meyerhof, H. P. Hülskötter, Qiang Dai, J. H. McGuire, and Y. D. Wang, Phys. Rev. A **44**, 5907 (1991).
[12] H. P. Hülskötter, W. E. Meyerhof, E. Dillard, and N. Guardala, Phys. Rev. Lett. **63**, 1938 (1989).
[13] D. H. Lee, T. J. M. Zouros, J. M. Sanders, P. Richard, J. M. Anthony, Y. D. Wang, and J. H. McGuire, Phys. Rev. A **46**, 1374 (1992).
[14] E. C. Montenegro and W. E. Meyerhof, Phys. Rev. A **44**, 7229 (1991).
[15] E. C. Montenegro and W. E. Meyerhof, Phys. Rev. A **46**, 5506 (1992).
[16] H. Tawara and A. Russek, Rev. Mod. Phys. **45**, 178 (1973).
[17] M. E. Rudd, Y.-K. Kim, D. H. Madison, and J. W. Gallagher, Rev. Mod. Phys. **57**, 965 (1985).
[18] M. B. Shah, T. V. Goffe, and H. B. Gilbody, J. Phys. B **10**, L723 (1977).
[19] M. E. Rudd, T. V. Goffe, A. Itoh, and R. D. Dubois, Phys. Rev. A **32**, 829 (1985).
[20] M. Sataka, A. Yagishita, and N. Nakai, J. Phys. B **23**, 1225 (1990).
[21] H. Atan, W. Steckelmacher, and M. W. Lucas, J. Phys. B **24**, 2559 (1991).
[22] R. D. DuBois, Phys. Rev. A **39**, 4440 (1989).
[23] N. V. de Castro Faria, F. L. Freire Jr., and A. G. de Pinho, Phys. Rev. A **37**, 280 (1988).
[24] F. Salvat, J. D. Martinez, R. Mayol, and J. Parellada, Phys. Rev. A **36**, 467 (1987).

[25] K. L. Bell, V. Dose, and A. E. Kingston, J. Phys. B **3**, 129 (1970).
[26] A. K. Edwards, R. M. Wood, and R. L. Ezell, Phys. Rev. A **42**, 1799 (1990).
[27] V. A. Sidorovitch, V. S. Nicolaev, and J. H. McGuire, Phys. Rev. A **31**, 2193 (1985); see also J. H. McGuire, Adv. At. Mol. Opt. Phys. **29**, 217 (1992).
[28] J. M. Hansteen, O. M. Johnsen, and L. Kocbach, At. Data Nucl. Data Tables **15**, 315 (1975).
[29] E. C. Montenegro, W. S. Melo, W. E. Meyerhof, and A. G. de Pinho, Phys. Rev. Lett. **69**, 3033 (1992).
[30] R. D. DuBois and S. Manson, Phys. Rev. A **42**, 1222 (1990).
[31] O. Heil, R. D. DuBois, R. Maier, M. Kuzel, and K.-O. Groeneveld, Z. Phys. D **21**, 235 (1991).
[32] O. Heil, R. D. DuBois, R. Maier, M. Kuzel, and K.-O. Groeneveld, Phys. Rev. A **45**, 2850 (1992).
[33] J. Wang, C. O. Reinhold, and J. Burgdörfer, Phys. Rev. A **45**, 4507 (1992).
[34] D. H. Jakubassa-Amundsen, Z. Phys. D **22**, 701 (1992).
[35] E. C. Montenegro, Nucl. Instrum. Methods B (to be published).